49th AIAA Aerospace Sciences Meeting including the New Horizons Forum and Aerospace Exposition
4 - 7 January 2011, Orlando, Florida
AIAA 2011-206

Evaluation of Flame-Prolongation of ILDM and Flamelet Tabulated Chemistry Approaches for Laminar Flames

Pradeep K. Jha* and Clinton P. T. Groth†
University of Toronto Institute for Aerospace Studies
4925 Dufferin Street, Toronto, Ontario, Canada, M3H5T6

The present study considers the performance of tabulation methods for numerical simulation of complex chemical kinetics in laminar combusting flows and compares their predictions to results obtained by direct calculation. Two tabulation methods are considered: the Flame Prolongation of Intrinsic low-dimensional manifold (FPI) method and Steady Laminar Flamelet Model (SLFM). The FPI method is of current interest as it is a potentially unifying approach capable of dealing with both premixed and non-premixed flames for gaseous fuels. SLFM tabulation methods are popular for non-premixed flames and form a good basis for comparing the performance of the FPI approach. The performance of each method is also evaluated by comparing the results to the direct simulation of the laminar flames using two chemical kinetic schemes: simplified chemistry involving five species and one reaction and detailed chemistry involving 53 species and 325 reaction steps. As part of the evaluation process, the computational cost of each method is also assessed. The laminar flames considered in this study include: freely propagating laminar premixed flames, a two-dimensional axisymmetric methane-air opposed-jet diffusion flame, and a two-dimensional axisymmetric methane-air co-flow diffusion flame. Both tabulation methods are implemented in a parallel adaptive mesh refinement (AMR) framework for solving the complete set of governing partial differential equations. These equations are solved using a fully-coupled finite-volume formulation on body-fitted multi-block quadrilateral mesh. Significant improvements in terms of reduced computational requirements, as measured by both storage and processing time, are demonstrated for the tabulated methods.

Nomenclature

α	scalar value
χ	scalar dissipation rate of mixture fraction
δ_{ij}	Kronecker delta function
$\dot{\omega}_k$	mass reaction rate of species k produced by the chemical reactions
$\dot{\omega}_{Y_c}$	reaction rate of Y_c (sum of the reaction rates of all the species defining Y_c)
λ	mixture thermal conductivity
μ	molecular viscosity depending on fluid properties
ϕ	equivalence ratio
ρ	mixture density
τ	viscous force tensor
AW_j	atomic weight of species j
MW_j	molecular weight of species j
θ	azimuthal coordinate of the axisymmetric frame
φ	any thermodynamic quantity of the flow
$\varphi_{F,o}$	value of φ in the fuel stream
$\varphi_{O,o}$	value of φ in the oxidizer stream

*Ph.D. Candidate, jhapk@utias.utoronto.ca.
†Professor, groth@utias.utoronto.ca, Senior Member AIAA.

$\vec{\mathcal{J}}^k$	molecular diffusive flux of the species k
$\vec{g}$	body force vector
$\vec{q}$	molecular heat flux vector
$\vec{q}$	molecular heat flux vector
$\vec{u}$	velocity vector
c	progress variable, $Y_c(\phi, x)/{Y_c}^{\mathrm{EQ}}(\phi, x)$
C_p	gas specific heat at constant pressure
D_f	diffusion coefficient of $f = \lambda/\rho/C_p$
D_k	molecular diffusivity of the species k relative to the main species
D_{Y_c}	diffusion coefficient of $Y_c = \mu/\rho/Sc_{Y_c}$
e	specific total energy $(u_i u_i/2 + h - p/\rho)$
h	internal energy $\sum_{k=1}^{N} Y_k h_k$
h_k	absolute internal enthalpy for species k
M	number of species in the reduced set
N	total number of species
n_{C_j}	number of carbon atom in species j
p	pressure
r	radial coordinate of the axisymmetric frame
R_k	gas constant of species k
s	Stoichiometric oxidizer-fuel mass ratio
Sc_k	Schmidt number of species k
Sc_{Y_c}	Schmidt number of $Y_c = 1.0$
T	mixture temperature
x	spatial coordinate in the direction normal to the flame front
Y_k	mass fraction of species k
z	axial coordinate of the axisymmetric frame
${Y_c}^{\mathrm{EQ}}$	Y_c value in the burnt state (or equilibrium) of laminar-premixed flames
f	mixture fraction
Y_c	progress of reaction
Da	Damköhler number

I. Introduction

A major challenge in the simulation of combustion processes is the modelling and evaluation of reaction rates for accurately representing chemical kinetics. Direct numerical simulations (DNS) of large complex reaction mechanisms place heavy demands on computational resources in terms of processor time, memory and storage requirements. This has prompted researchers to consider computationally efficient approaches for modelling the chemical kinetics without significantly compromising the quality of results. Although not fully inclusive, the computationally efficient techniques for the treatment of complex chemistry in combustion processes can be broadly categorized into two groups:[1] (i) chemical reduction techniques; and (ii) flamelet approaches. The *in Situ* Adaptive Tabulation (ISAT) approach proposed by Pope,[2] based on the generation of look-up tables for chemical kinetics during direct simulations, falls somewhat outside this classification, but the classification is still useful nonetheless.

Chemical Reduction Techniques (CRT) are based on the observation that chemical processes are mainly determined by a small number of slow reactions. These methods assume that species involved in fast reaction processes are in a near quasi-equilibrium steady state. Computational savings are garnered by tracking only the finite-rate reactions and species involved in slow processes. CRT differ from each other mainly in how the fast and slow processes are determined and handled. The Systematic Reduction Method (SRM), as discussed in the review by Peters[3] invokes a steady-state assumption for species involved in fast chemical processes. This however involves a detailed study of all reaction steps and time scales, which can become quite involved for fuels with complex molecular structure.[4] The Computational Singular Perturbation (CSP) method proposed by Lam and Goussis[5] examines the Jacobian of the local chemical source terms to identify slow processes. CSP is quite accurate; however, slow processes are calculated dynamically and the number of steady-state variables varies continuously during the simulation, which can make the method computationally

expensive. The Intrinsic Low Dimensional Manifold (ILDM) approach, proposed by Mass and Pope,[6] is based on the analysis of the eigenstructure of the source Jacobian to identify slow chemical processes. Based on this eigensystem analysis, a small subset of variables is identified which evolves slowly during combustion. These variables are then used to generate pre-computed look-up tables to be used during simulations for evaluating chemical kinetics. The ILDM method has been shown to fail in regions of flow where diffusion processes are as important as chemical processes and it generally does not yield good results in low temperature regions of flames as fast time scales have been neglected. The Trajectory Generated Low Dimensional Manifold (TGLDM) is based on the same principles as the ILDM method, however, instead of the chemical reacting system, the TGLDM system computes a manifold using trajectories.[7] The trajectory is the path the system takes through composition space from the initial point to the chemical equilibrium composition. TGLDM methods have the advantage over ILDM methods that they guarantee convergence and that the reaction vector is always tangent to the trajectory. A disadvantage is that it is not yet clear how one can incorporate the effects of diffusion on the manifold with TGLDM methods, as has been done with ILDM methods.[8]

Flamelet approaches assume that the local chemical structure of a flame is independent of the physical complexity of the surrounding flow. Pre-generated solutions of chemical composition for simple flames are used to predict local chemical composition in more complex situations using solution mapping procedures and functions. Flamelet methods have become popular for the treatment of diffusion flames over the last 10-15 years. Several past attempts have been made to study the chemical properties of a diffusion flame as a function of one conserved scalar (Bilger,[9] Libby and Williams[10]). In the Steady Laminar Flamelet Model (SLFM) of Peters,[11] pre-computed detailed chemistry solutions of one-dimensional counter flow flames are used for the simulation of more general diffusion flames. For this, all flame properties at any point in the flow are expressed in terms of mixture fraction and another scalar characterizing the dissipation of the mixture fraction.[11] Subsequent follow-on studies have considered the application of this formulation.[12–14] Smooke *et al.*[15] and Nishioka *et al.*[16] have compared multi-dimensional laminar diffusion flame simulation results to one-dimensional counter-flow flames and reported that there is good agreement between the structure of the two flames. Smooke *et al.*[15] observed that the flamelet model yields poor predictions for some species concentrations in fuel-rich regions. In a recent study of the flamelet model for laminar flames, Liu *et al.*[14] compared directly-calculated solutions with those of the flamelet approach for a co-flow diffusion flame and noted that numerical results depend quantitatively on the definition of dissipation rate and mixture fraction.

Flame-Prolongation of ILDM (FPI) and Flame-Generated Manifold (FGM) are two tabulated approaches developed independently by Gicquel *et al.*[17] and Oijen *et al.*,[4] respectively. The two methods are conceptually similar and can be viewed as hybrids of the CRT and flamelet methods discussed above. They both use pre-tabulated solutions of flames that have simplified flow geometry, which are subsequently used for the simulation of more complex flames. A controlling parameter, called the progress of reaction variable is introduced to define the mapping between the tabulated solutions and local solutions within a combustion simulation. When detailed solutions of one-dimensional laminar premixed flames are used as the basis for the tabulation in the FPI approach, both FPI and FGM are essentially identical. The primary differences between the methods are then technical and relate simply to how the tabulated data is constructed and accessed. The FGM approach is based on tabulating data as a function of enthalpy and progress of reaction variable, while FPI stores data as a function of the mixture fraction and progress of reaction variable.

The FPI and FGM schemes are currently of great interest as they are potentially unifying approaches which can be applied to the full range of flames, i.e., premixed, partially-premixed, and non-premixed flames. For laminar premixed flames, Gicquel *et al.*[17] and Oijen *et al.*[4] indicated that their respective approaches are much faster than directly performing calculations with detailed chemistry. The FPI method was extended to diffusion flames by Vervisch *et al.*[18] and for non-adiabatic flames by Fiorina *et al.*[19] Fiorina *et al.*[20] subsequently also assessed the performance of the FPI method for one-dimensional counter-flow flames. More recently, Galpin *et al.*[21] have examined different ways in which the FPI approach can be coupled to reactive flow solution methods. Additionally, both FPI and FGM have been successfully applied in computations of complex turbulent combusting flows.[21–25]

Although the FPI and flamelet methods have already been developed and applied to turbulent combusting flows as indicated above, it can still be very instructive to consider their application and performance to laminar flames. Such studies provide valuable insight into understanding and interpreting the capabilities of these approximate techniques when applied to turbulent flames, which is of course the ultimate objective. Moreover, as the FPI has been shown to have considerable potential when applied to various combustion regimes, i.e., to autoignition,[24] lifted flames,[25] and unsteady flames, a performance review of the method

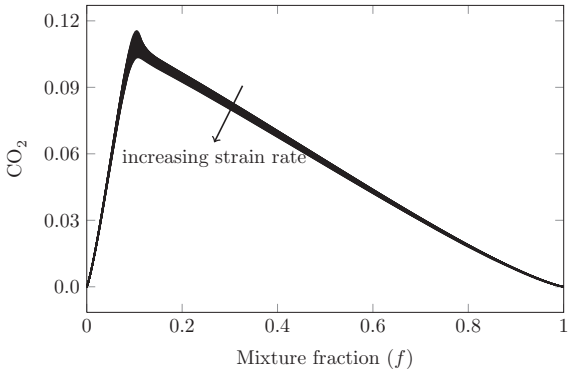

Figure 1: Variation of concentration of CO_2 in the mixture fraction space for different values of the strain rate.

for laminar flames would seem particularly important and timely. With this viewpoint, the performance of FPI and the SLFM schemes are both compared herein for selected laminar flames. The accuracy and computational costs of the FPI and SLFM methods are assessed and discussed.

II. Tabulation Methods for Chemical Kinetics

II.A. Steady Laminar Flamelet Model (SLFM)

The SLFM approach expresses all of the local thermochemical properties of a diffusion flame as a function of a single conserved scalar. This approach is based on the observation that the reaction zone in diffusion flames are limited to a thin region where reactants mix with each other in a stoichiometric ratio. Hence, the local instantaneous reaction zone structure is assumed to be the same as that of a quasi-steady one-dimensional laminar flame.[11]

The mixing at any point in the flow is defined by a scalar field called the mixture fraction, f, defined as[26]

$$f = \frac{\text{mass of material having its origin in the fuel stream}}{\text{mass of mixture}} \tag{1}$$

The values of the mixture fraction vary from zero in the oxidizer feed to one in the fuel feed. Peters[11] has previously derived the flamelet equation for unity Lewis numbers of chemical species as

$$\frac{\partial Y_i}{\partial t} = \rho \frac{\chi}{2} \frac{\partial^2 Y_i}{\partial f^2} + \dot{\omega}_i, \quad (i = 1, \ldots, N) \tag{2}$$

where

$$\chi = 2 D_f \frac{\partial f}{\partial x_i} \frac{\partial f}{\partial x_i} \tag{3}$$

and where χ is the scalar dissipation rate, $D_f = \lambda/\rho/C_p$ is the diffusion coefficient of f, and C_p is the gas specific heat at constant pressure. The diffusion coefficient of mixture fraction, D_f, is chosen to be the same as the thermal diffusivity of the mixture. This is justified by the fact that under certain simplifying assumptions the energy and mixture fraction transport equation take on similar forms.[26] The steady-state form of Equation (2) can be solved numerically using well developed methodologies and software, such as provided by Cantera,[27] to obtain steady-state solutions for counter-flow diffusion flames for different strain rate values. In the present work, the strain rate value is defined as the velocity gradient at the stagnation point of the counter-flow flame. Solutions for a series of strain rates, ranging from small values (near equilibrium) to very large values (approaching the quenching limit) are calculated using the Cantera software package. While Equation (2) shows that the value of χ varies at every position in the laminar flame solution, a single characteristic value of the scalar dissipation rate is chosen to represent the solution for each strain rate value. Since most of the chemical activity occurs in the vicinity of the stoichiometric point of the flame, it is usually adequate to take the value of the scalar dissipation rate at the stoichiometric mixture fraction, χ_{st}, as the characteristic value.[11,14] Some authors also use the value of χ at the maximum temperature as

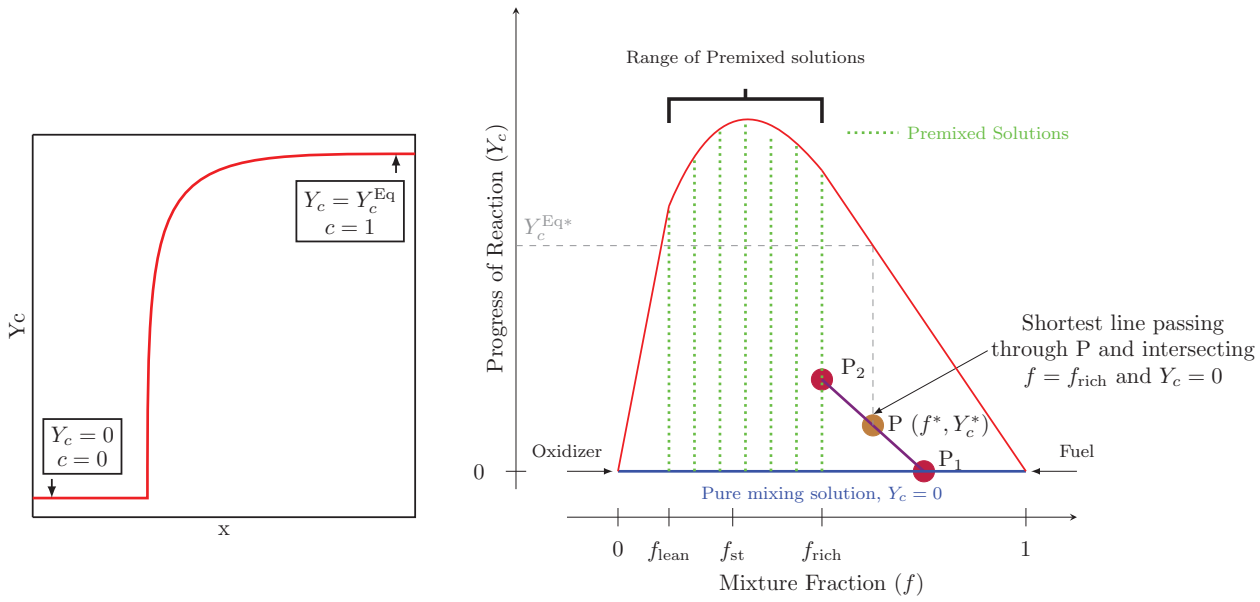

(a) Schematic representation of Y_c and c for 1D premixed flames

(b) Solution procedure for FPI in the Y_c-f space

Figure 2: Schematic diagrams illustrating algorithm used for interpolation of FPI tabulated flamelet data.

the characteristic rate.[28] For the methane-air flames being studied in this paper, these values are virtually identical.

The counter-flow diffusion flame solutions are stored in a flamelet library such that any thermochemical quantity, φ, can be retrieved and expressed as $\varphi^{\mathrm{FL}} = \varphi(f, \chi_{st})$. For general combusting flows, the balance equation for the mixture fraction, f, is then solved instead of the full set of species continuity equations, and the local scalar dissipation rate, χ, is calculated at each point using Equation (3). Local values of f and χ are used to obtain the local chemical composition from the flamelet library using a bi-linear interpolation procedure. Peters[11] mentions that NOx and soot particles are particularly sensitive to χ, but as the present work does not consider the formation of either of these pollutants, the variation in species concentration as a function of scalar dissipation rate should not be a significant factor. Figure 1 shows the change in concentration of CO_2 for different strain rate values. Similar behaviour is also observed for other thermochemical quantities. The effect of the number of tabulated strain rates is discussed further in Section IV.C.

For the methane-air flames of interest here, two SLFM tabulation approaches are considered:

- **Approach 1:** The local values of f and χ are used to obtain mass fractions from the flamelet library. A consistent solution for the mixture temperature, T, is obtained by solving the energy equation.
- **Approach 2:** Both mass fractions and temperature, T, are read from the flamelet library as a function of local value of f and χ. The energy equation is not solved.

The results and performance of both of these two approaches are discussed in Section IV.

II.B. Flame Prolongation of ILDM (FPI)

II.B.1. Tabulation of Detailed Chemistry Solutions

In the FPI approach, every thermochemical quantity, φ, is expressed as a function of two independent variables: the mixture fraction, f, and progress of reaction variable, Y_c. Using the definition of f from Equation (1), for a pure-mixing/non-reacting situation the local value of any quantity, φ, can be expressed as a linear function of f using the relation

$$\varphi = f\varphi_{F,o} + (1 - f)\varphi_{O,o} \tag{4}$$

where $\varphi_{F,o}$ is the value of φ in the fuel stream and $\varphi_{O,o}$ is the value of φ in the oxidizer stream. For a given equivalence ratio, ϕ, defined by

$$\phi = \frac{(\text{Air/Fuel})_{\text{stoic}}}{(\text{Air/Fuel})} \tag{5}$$

all flame properties of a one-dimensional laminar premixed flame can be expressed as

$$\varphi = \varphi(\phi, x) \tag{6}$$

where x is the spatial coordinate in the direction normal to the flame front. Using Equation (4) with Equation (5), f can then be expressed uniquely as a function of ϕ as

$$f(\phi) = \frac{\phi}{\left(\phi + s\frac{Y_{F,o}}{Y_{O,o}}\right)} \tag{7}$$

where s is the stoichiometric oxidizer-fuel mass ratio. For simple hydrocarbons, Y_c can be defined as a linear combination of the species mass fractions, Y_i, and written as

$$Y_c(\phi, x) = \sum_{j=1}^{N} \alpha_j Y_j(\phi, x) \tag{8}$$

such that there is a one-to-one correspondence between x and Y_c, for a given equivalence ratio. Eliminating the spatial coordinate, x, using Equations (6) and (8), the final FPI tabulation is carried out as follows:

$$\varphi^{\text{FPI}} = \varphi(\phi, x) = \varphi(f(\phi), Y_c(x)) \tag{9}$$

The choice of Y_c varies from fuel to fuel. For methane-air flames, Fiorina *et al.*[19] propose that a linear combination of the mass fraction of CO and CO_2 is a good choice for Y_c. For practical considerations,[18] a normalized value of Y_c, called the progress variable, c, is introduced. The progress variable, as illustrated in Figure 2a, is defined as

$$c = \frac{Y_c(\phi, x)}{{Y_c}^{\text{EQ}}(\phi, x)} \tag{10}$$

where ${Y_c}^{\text{EQ}}$ is the value of Y_c in the burnt state of the laminar-premixed flame. The final FPI look-up table for laminar flames is then of the form

$$\varphi^{\text{FPI}} = \varphi(f, c) \tag{11}$$

As with the SLFM, the Cantera package,[27] based on GRI-Mech 3.0 mechanism, is again used to obtain detailed chemistry solutions for one-dimensional premixed flames for different equivalence ratios within the flammability limits of premixed flames.

For premixed flames, a number of studies have reported on the validity of the preceding approach.[19,20,29] However, for diffusion flames, the mixture fraction values can lie outside the flammability limits of premixed flames and take on values any where from zero to one. To calculate the mass fractions for points lying outside the range of valid premixed flame solutions, a linear interpolation is performed between the rich/lean flammability limit solution and the pure-mixing solution given by Equation (4). This approach, illustrated in Figure 2b, differs somewhat from methods proposed previously.[18,30] The reaction rates are also set to zero outside the premixed flame flammability limits.

II.B.2. Coupling Tabulated Data with Reactive Flow Solution Algorithm

The FPI table size can be an important concern and can tax available computer memory when performing practical calculations, especially when dealing with non-premixed turbulent flames. Galpin *et al.*[31] have shown that of the 53 GRI-Mech 3.0 mechanism species, only 7 species: CH_4, O_2, CO_2, CO, H_2O, H_2 and N_2, are needed to account for more than 99.5% of the total mass and energy of the mixture. Therefore, using the information for only these 7 species affords virtually a full description of the flame properties. However, in order to properly account for the elemental mass of the remaining species, additional species must also be tabulated. Careful studies have shown that H, OH and C_2H_2 are a good choice for these additional species in the case of methane-air flames.[31] Hence, the final look-up table in the current study stores data for a total of 10 species (7 major and 3 minor species).

Three approaches are considered here for coupling the FPI tabulated data to the reactive flow solution algorithm used here:

Approach	Tabulated	Species PDEs Solved	Methodology
1	Y_i, $\dot{\omega}_{Y_c}$	No	Get Y_i from table using $Y_i = Y_i(f, Y_c)$. Use Y_i directly in the solver.
2	$\dot{\omega}_i$, $\dot{\omega}_{Y_c}$	Yes	Get $\dot{\omega}_i$ from table using $\dot{\omega}_i = \dot{\omega}_i(f, Y_c)$. Use $\dot{\omega}_i$ in species PDEs for reaction rate source term.
3	Y_i, $\dot{\omega}_{Y_c}$	Yes	Get Y_i from table. Reconstruct $\dot{\omega}_i$ using $\dot{\omega}_i \approx \dot{\omega}_{Y_c} \frac{\partial Y_i}{\partial Y_c}$. Use these $\dot{\omega}$ values in species PDEs.

Table 1: Different ways of coupling the FPI look-up table to the flow solver. In all methods, $\dot{\omega}_{Y_c}$ for Y_c transport equation is obtained from the table.

- **Approach 1 – Tabulated Mass Fractions**: The look-up table stores the mass fractions of the reduced set of species. The mass fractions of the major species are used directly from the pre-computed solutions whereas the mass fractions of minor or additional species, such as C_2H_2 and H_2, are calculated by ensuring atomic mass conservation.[21] For example, when the detail chemistry solution of all 53 species is known, the conservation of atomic mass of carbon atoms provides the following expression for calculating $Y_{C_2H_2}$ in the reduced set of species:

$$Y_{C_2H_2} = \frac{MW_{C_2H_2}}{n_{C_{C_2H_2}}} \left(\sum_{j=1}^{N} Y_j \frac{n_{C_j} AW_C}{MW_j} - \sum_{\substack{j=1 \\ j \neq C_2H_2}}^{M} Y_j \frac{n_{C_j} AW_C}{MW_j} \right) \tag{12}$$

  where N is the total number of species, M is the number of species in the reduced set, n_{C_j} is the number of carbon atom in species j, AW_j is the atomic weight of species j, and MW_j is the molecular weight of species j.

  Individual species transport equations are not solved. Instead, local values of f and Y_c are used to obtain the species concentrations from the table using bi-linear interpolation.

- **Approach 2 – Tabulated Reaction Rates**: The look-up table stores the reaction-rates of the reduced set of species. The reaction rates of the major species are used directly from the pre-computed solutions but the reaction rates of the additional minor species are evaluated by using atomic mass conservation.[21] For example, conservation of atomic mass of Carbon atoms gives the following expression for $\dot{\omega}_{C_2H_2}$:

$$\dot{\omega}_{C_2H_2} = -\frac{MW_{C_2H_2}}{n_{C_{C_2H_2}}} \sum_{\substack{j=1 \\ n_{C_j} \neq 0 \\ j \neq C_2H_2}}^{M} \frac{\dot{\omega}_j}{MW_j} \tag{13}$$

  The transport equations for the mass fractions of each species in the reduced set, both major and minor species, are solved. The tabulated reaction rates stored as a function of local values of f and Y_c are used in evaluating the chemical source terms appearing in the species transport equations.

- **Approach 3 – Tabulated Mass Fractions & Estimated Reaction Rates**: Highly diffusive species can have large gradient values. Resolving these high values using tabulated species mass fraction needs highly refined tables. A bridge between the above two approaches is to use a mass fraction look-up table, like Approach 1, and reconstruct the species reaction rates using this mass fraction data. Domingo *et al.*[23] have shown that in a laminar premixed flame, the source terms are related by

$$\dot{\omega}_i = \dot{\omega}_{Y_c} \left[\frac{\partial Y_i}{\partial Y_c} - \frac{1}{Da} \left(\frac{\partial^2 Y_i}{\partial {Y_c}^2} \right) \right] \tag{14}$$

  where Da is the Damköhler number. For fast chemistry and large values of Da, the second term can be neglected to yield the simplified expression

$$\dot{\omega}_i \approx \dot{\omega}_{Y_c} \frac{\partial Y_i}{\partial Y_c} \tag{15}$$

The species mass balance equations are then solved directly using the above expression. This approach avoids the need for a large number of tabulated values as in Approach 2 to account for the wide ranges in the magnitude of the reaction rates for the more diffusive species.

In all of the above approaches, the conservation equations for mass, momentum, energy, are solved along with transport equations for the mixture fraction and progress of reaction variable. Table 1 summarizes these approaches.

The FPI, and for that matter, the SLFM tabulation methods are both coupled to a density-based solution algorithm of the compressible form of the Navier-Stokes equations for a reactive mixture (the solution method and governing equation are summarized in the next section of the paper to follow). However, as all of the laminar flames considered in the present study are both steady and essentially isobaric, and radiation losses are not significant, the coupling of the tabulation methods with the solution algorithm was rather straightforward. The tabulations were performed for a single pressure (atmospheric pressure) and any small variations in pressure from the reference condition were ignored when using and accessing the tables. Nevertheless, for more general combustion processes involving non-adiabatic flames with acoustical phenomena and/or significant pressure variations, coupling of the tabulation methods to a compressible-flow solution method would be more involved and a multi-pressure tabulation procedure may be required. Issues of coupling of the FPI and SLFM methods to a solution algorithm for the governing flow equations is not the primary focus here. Galpin *et al.*[31] and the recent paper by Vicquelin *et al.*[32] discuss coupling of tabulated chemistry methods with various solution methods for the flow equations.

III. Governing Equations and Numerical Scheme

III.A. Navier-Stokes Equations for a Reactive Mixture

Neglecting soot formation and radiation transport, laminar flames can be fully described by the Navier-Stokes equations for a compressible, thermally-perfect, reactive mixture governing the conservation of mass, momentum, and energy for the mixture and the transport of mass for each of the individual species. The balance equations in tensor notation for a N-species reactive mixture are given by[33,34]

$$\frac{\partial \rho}{\partial t} + \frac{\partial}{\partial x_i}\left(\rho u_i\right) = 0 \tag{16}$$

$$\frac{\partial}{\partial t}\left(\rho u_i\right) + \frac{\partial}{\partial x_j}\left(\rho u_j u_i\right) = -\frac{\partial p}{\partial x_i} + \frac{\partial \tau_{ji}}{\partial x_j} + G_i \tag{17}$$

$$\frac{\partial}{\partial t}\left(\rho Y_k\right) + \frac{\partial}{\partial x_j}\left(\rho u_j Y_k\right) = -\frac{\partial \mathcal{J}_j^k}{\partial x_j} + \dot{\omega}_k \tag{18}$$

$$\frac{\partial}{\partial t}\left(\rho e\right) + \frac{\partial}{\partial x_j}\left[\rho u_j\left(e + \frac{p}{\rho}\right)\right] = \frac{\partial}{\partial x_j}\left(u_i \tau_{ij}\right) - \frac{\partial q_j}{\partial x_j} + u_i G_i \tag{19}$$

The molecular heat flux vector is given by

$$q_j = -\lambda \frac{\partial T}{\partial x_j} + \sum_{k=1}^{N} Y_k h_k u_j \tag{20}$$

The mixture pressure is given by the ideal gas law, $p = \sum_{k=1}^{N} \rho Y_k R_k T$. The fluid is assumed to be Newtonian and so the viscous stress tensor has the form

$$\tau_{ij} = \mu\left(\frac{\partial u_i}{\partial x_j} + \frac{\partial u_j}{\partial x_i}\right) - \frac{2}{3}\delta_{ij}\frac{\partial u_k}{\partial x_k} \tag{21}$$

Species molecular diffusivity is determined using Fick's law and given by

$$\mathcal{J}_j^k = -\frac{\mu}{\mathrm{Sc}_k}\frac{\partial Y_k}{\partial x_j} \tag{22}$$

where

$$\mathrm{Sc}_k = \frac{\mu}{\rho D_k} \tag{23}$$

In the expressions above, ρ is the mixture density, $\vec{u}$ is the velocity vector, p is the pressure, τ is the viscous force tensor, $\vec{g}$ is the body force vector, Y_k is the mass fraction of species k, $\dot{\omega}_k$ is the mass reaction rate of species k produced by the chemical reactions, $\vec{\mathcal{J}}^k$ is the molecular diffusive flux of the species k, e is the specific total energy $(u_i u_i/2 + h - p/\rho)$, h is the internal energy $\sum_{k=1}^{N} Y_k h_k$, h_k is the absolute internal enthalpy for species k, $\vec{q}$ is the molecular heat flux vector, R_k is the gas constant of species k, T is the mixture temperature, λ is the mixture thermal conductivity, μ is the molecular viscosity depending on fluid properties, δ_{ij} is the Kronecker delta function, Sc_k is the Schmidt number of species k, and D_k is the molecular diffusivity of the species k relative to the main species.

III.B. Additional Balance Equations

Both the FPI and the SLFM approach use the mixture fraction variable, f, to obtain the chemical composition at any point in the flow from the look-up table. The FPI tabulation is also dependent on another parameter called the progress of reaction, Y_c. The balance equations for these two scalar variables are given by

$$\frac{\partial}{\partial t}(\rho f) + \frac{\partial}{\partial x_i}(\rho u_i f) = \frac{\partial}{\partial x_i}\left(\rho D_f \frac{\partial f}{\partial x_i}\right) \tag{24}$$

$$\frac{\partial}{\partial t}(\rho Y_c) + \frac{\partial}{\partial x_i}(\rho u_i Y_c) = \frac{\partial}{\partial x_i}\left(\rho D_{Y_c} \frac{\partial Y_c}{\partial x_i}\right) + \rho \dot{\omega}_{Y_c} \tag{25}$$

where $D_{Y_c} = \mu/\rho/Sc_{Y_c}$ is the diffusion coefficient of Y_c, $\dot{\omega}_{Y_c}$ is the reaction rate of Y_c (sum of the reaction rates of all the species defining Y_c), and Sc_{Y_c} is the Schmidt number for the progress variable which is taken to have a constant value of unity herein.

The source term, $\dot{\omega}_{Y_c}$, appears in Equation (25). In FPI tabulation, this value is also stored in the look-up table as a function of Y_c and f. The value is obtained from the table along with the species mass fraction and/or reaction rates, as a function of local values of Y_c and f.

III.C. Conservation Form of Equations

For two-dimensional axisymmetric flows, the preceding equations governing a reactive compressible mixture can be re-expressed using vector notation as

$$\frac{\partial \mathbf{U}}{\partial t} + \frac{\partial}{\partial r}(\mathbf{F} - \mathbf{F}_v) + \frac{\partial}{\partial z}(\mathbf{G} - \mathbf{G}_v) = \frac{1}{r}(\mathbf{S}_\phi + \mathbf{S}_{\phi v}) + \mathbf{S} \tag{26}$$

where $\mathbf{U}$ is the vector of conserved variables given by

$$\mathbf{U} = \left[\ \rho,\ \rho v_r,\ \rho v_z,\ \rho e,\ \rho Y_1,\ \ldots,\ \rho Y_n,\ \rho f,\ \rho Y_c\ \right]^{\mathrm{T}} \tag{27}$$

and r and z are the radial and axial coordinates of the axisymmetric frame. The inviscid and viscous radial flux vectors, $\mathbf{F}$ and $\mathbf{F}_v$, are

$$\mathbf{F} = \left[\ \rho v_r,\ \rho v_r^2 + p,\ \rho v_r v_z,\ (\rho e + p) v_r,\ \rho v_r Y_1,\ \ldots,\ \rho v_r Y_n,\ \rho v_r f,\ \rho v_r Y_c\ \right]^T \tag{28}$$

$$\mathbf{F}_v = \left[\ 0,\ \tau_{rr},\ \tau_{rz},\ v_r\tau_{rr} + v_z\tau_{rz} - q_r,\ -\mathcal{J}_r^1,\ \ldots,\ -\mathcal{J}_r^n,\ \rho D_f \tfrac{\partial f}{\partial r},\ \rho D_{Y_c} \tfrac{\partial Y_c}{\partial r}\ \right] \tag{29}$$

and the inviscid and viscous axial flux vectors, $\mathbf{G}$ and $\mathbf{G}_v$, are

$$\mathbf{G} = \left[\ \rho v_z,\ \rho v_r v_z,\ \rho v_z^2 + p,\ (\rho e + p) v_z,\ \rho v_z Y_1,\ \ldots,\ \rho v_z Y_n,\ \rho v_z f,\ \rho v_z Y_c\ \right]^T \tag{30}$$

$$\mathbf{G}_v = \left[\ 0,\ \tau_{zr},\ \tau_{zz},\ v_r\tau_{rr} + v_z\tau_{rz} - q_r,\ -\mathcal{J}_z^1,\ \ldots,\ -\mathcal{J}_z^n,\ \rho D_f \tfrac{\partial f}{\partial z},\ \rho D_{Y_c} \tfrac{\partial Y_c}{\partial z}\ \right]^T \tag{31}$$

The source terms, $\mathbf{S}_\phi$ and $\mathbf{S}_{\phi v}$, are the inviscid and viscous source vectors associated with the axisymmetric geometry, respectively. The source vector, $\mathbf{S}$, contains terms related to the finite rate chemistry and body force due to gravity. These three source vectors have the respective forms:

$$\mathbf{S}_\phi = \left[\; -\rho v_r, \, -\rho v_r^2, \, -\rho v_r v_z, \, -\rho v_r(\rho e + p), \, -\rho v_r Y_1, \, \ldots, \, -\rho v_r Y_n, \, -\rho v_r f, \, -\rho v_r Y_c \; \right]^T \tag{32}$$

$$\mathbf{S}_{\phi \mathbf{v}} = \left[\; 0, \, \tau_{rr} - \tau_{\theta\theta}, \, \tau_{rz}, \, v_r \tau_{rr} + v_z \tau_{rz} - q_r, \, -\mathcal{J}_r^1, \, \ldots, \, -\mathcal{J}_r^n, \, \rho D_f \frac{\partial f}{\partial r}, \, \rho D_{Y_c} \frac{\partial Y_c}{\partial r} \; \right]^T \tag{33}$$

$$\mathbf{S} = \left[\; 0, \, 0, \, \rho g_z, \, \rho v_z g_z, \, \rho \dot{\omega}_1, \, \ldots, \, \rho \dot{\omega}_n, \, 0, \, \rho \dot{\omega}_{Y_c} \; \right]^T \tag{34}$$

III.D. Parallel Block-Based AMR Finite-Volume Solution Method

For the direct-calculation of the laminar flames considered here, the preceding system of non-linear conservation laws governing the a compressible, thermally-perfect, reactive mixture are solved numerically using a parallel, fully-coupled, finite-volume scheme with block-based AMR on body-fitted, multi-block, quadrilateral computational mesh previously developed by Groth and co-workers.[35–38] The scheme makes use of piecewise limited linear reconstruction and a Riemann-solver-based flux functions to determine the inviscid flux. A second-order diamond-path discretization method is used for the viscous fluxes. The solution of the fully-coupled non-linear ODEs are obtained via a method of lines approach. This fully-coupled density-based approach for the compressible-form of the Navier-Stokes equations uses low-Mach-number preconditioning to deal with the low-speed flows associated with the laminar flames. Thermodynamic and transport properties for the reactive mixture, along with chemical kinetic rates, are evaluated using Cantera,[27] an open-source software package for chemically-reactive flows. For the methane-air flames considered in this study, results were obtained for two reaction mechanisms: a simplified one-step, five-species, chemical kinetic scheme proposed by Westbrook and Dryer[39] and detailed Gri-Mech 3.0 mechanism involving 53 species and 325 reactions.[40] A more complete description of the solution methodology used here is given in the papers by Northrup and Groth,[35] Charest *et al.*,[38] and Gao *et al.*[41]

The parallel, block-based, AMR scheme described above has been modified to allow for the use of the SLFM and FPI tabulated-chemistry methods of primary interest here and to perform the table generation. Coupling of these two tabulation methods to the solution algorithm is described in Sections II.A and II.B.2 above.

IV. Numerical Results and Discussions

IV.A. Laminar Premixed Flames

The performance and predictive capabilities of the FPI approaches are first investigated for stationary one-dimensional laminar premixed methane-air flames with equivalence ratios ranging from ϕ=0.4 to ϕ=2.0. A two-dimensional rectangular grid with dimensions 50 mm by 0.65 mm was used for this case. A highly stretched mesh of size 2 cells by 160 cells was used. The finest grid size near the flame front was of the order of 0.01 mm and the coarse grid size near the boundary was of the order of 1.2 mm.

The Cantera package was used to obtain solutions for one-dimensional laminar premixed flames needed for generating the FPI look-up table. Sixty-four solutions corresponding to different equivalence ratios in the flammability limit ranging from ϕ=0.4 to ϕ=2.0 were used. For each value of ϕ, the premixed flame solution contained 155 points in c-space. These points were non-uniformly distributed such that there were more points in regions of high gradients.

Figures 3a and 3b compare the results obtained using the three FPI approaches to directly-calculated results obtained using both the one-step mechanism and the full GRI-Mech 3.0 mechanism without any tabulation. Both the predicted flame speed and burnt-gas or flame temperature are shown. Figure 3a shows extremely good agreement between the laminar flame speeds predicted by all three FPI approaches and the detailed chemistry solution using Cantera over the entire flammability range. This is a significant improvement over the results obtained from the simplified one-step mechanism, which fails to predict the right flame speed for much of the flammability range. It should be noted, that all of the FPI predictions

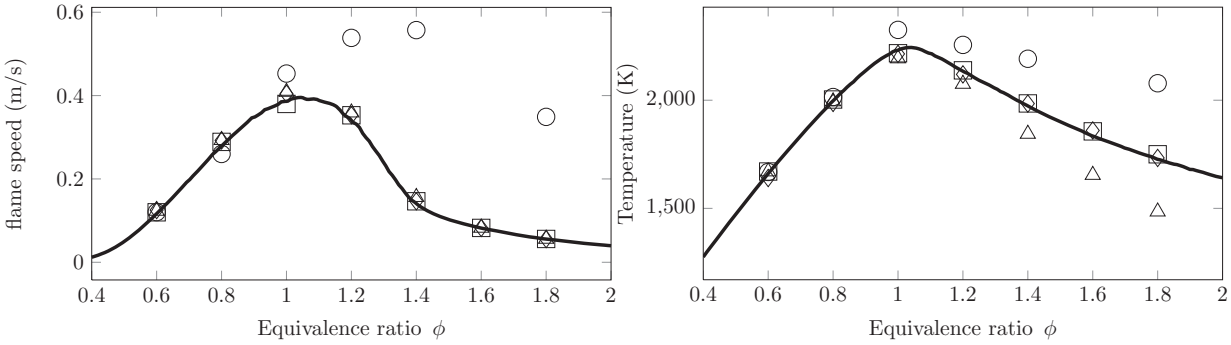

(a) Predicted flame-speed versus ϕ.

(b) Predicted flame temperature versus ϕ.

Figure 3: Predicted solutions of one-dimensional laminar methane-air premixed flames. Line: Detailed Chemistry, square: FPI-Approach 1, triangle: FPI-Approach 2, diamond: FPI-Approach 3, circle: one-step mechanism.

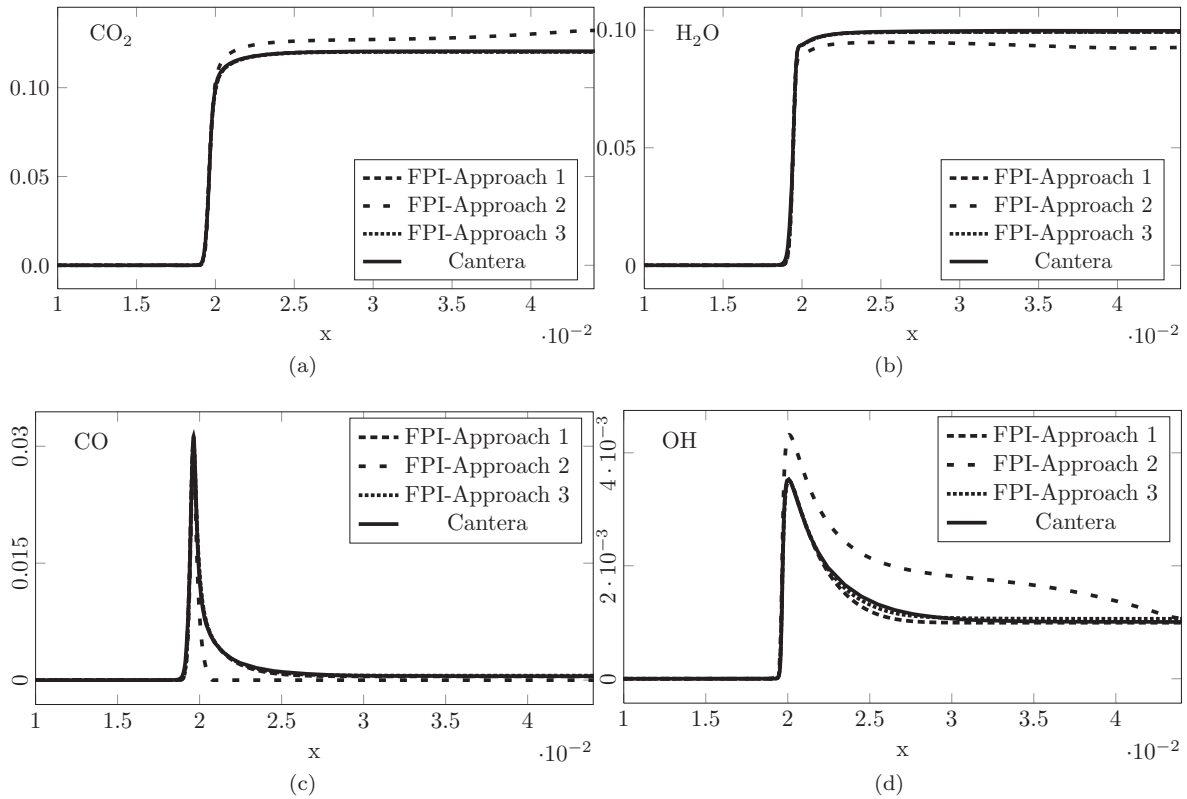

Figure 4: Predicted variation of species concentrations through flame obtained using the three different FPI coupling schemes for $\phi = 0.8$.

were made using the reduced set of ten species, as discussed earlier in Section II.B. These results show that the reduction procedure is a valid simplification for controlling the size of the look-up table, as was shown previously by other authors.[23,31] However, the comparisons of flame temperature in Figure 3b clearly show the differences between the reaction rate tabulation method and mass fraction tabulation methods. FPI-Approach 2 under-predicts the burnt gas temperature for rich flame conditions. Figure 4 takes a closer look at the species mass fractions predicted by each FPI-Approach. The results of the figure show that the mass fractions of some minor species, like OH and CO, are poorly predicted by FPI-Approach 2. This occurs because the magnitude of the reaction rate gradients for these species are very large near the flame

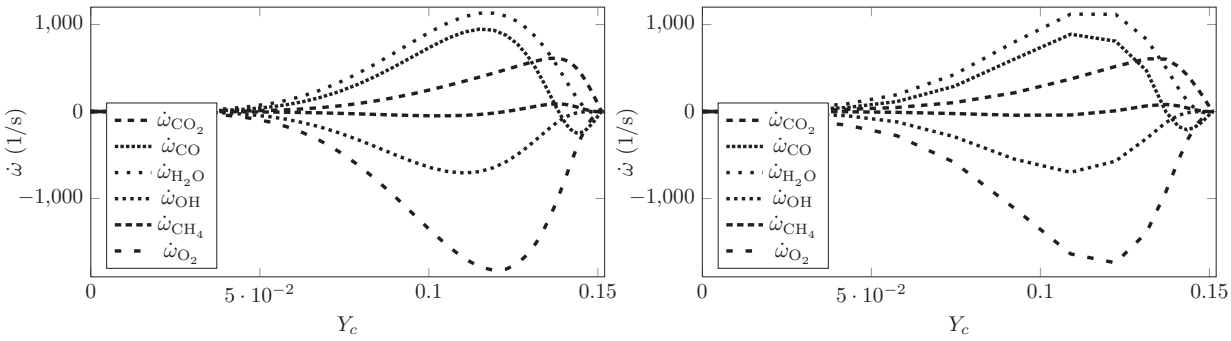

(a) Detail chemistry predictions.

(b) FPI predictions.

Figure 5: Predicted variations of the reaction rates for different species within a one-dimensional laminar methane-air premixed flame.

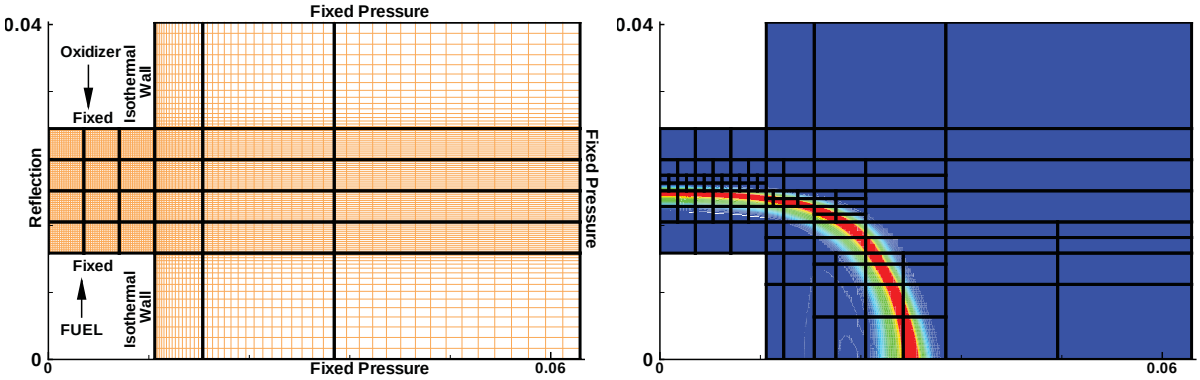

(a) Initial Coarse Grid - 30 blocks.

(b) Grid after 2 levels of refinement - 120 blocks.

Figure 6: Illustration of adaptive Mesh Refinement (AMR) scheme for laminar counter-flow methane-air flame.

front and the discretization of c-space using 155 points is not sufficient to accurately capture the solution of minor species. It is for this reason that only FPI-Approaches 1 and 3 have been used in the remainder of the laminar flame validation cases to follow.

As FPI-Approach 3 is based on the reconstruction of reaction rates, it is also of interest to show how well the method predicts the reaction rate values for different species for the laminar premixed case. Figure 5 compares the reaction rate predicted by Cantera and the reconstructed reaction rate predicted by FPI-Approach 3. The predictions are almost exact, both in their shape and magnitude.

IV.B. Laminar Counter-Flow Methane-Air Flame

The SLFM approach is based on the assumption that for the same value of a conserved scalar at any point in the flow, the local structure of a general laminar diffusion flame is the same as that of any simplified laminar diffusion flame. Most commonly, the detailed chemistry solutions of simplified one-dimensional counter-flow diffusion flames are used to generate flamelet libraries which can be used for more complex flow geometries, as proposed by Peters.[11] It is therefore important to compare the performance of the FPI approach with SLFM for predicting the counter-flow diffusion flames, as FPI uses the premixed flamelet solutions for predicting diffusion flames.

The experimental set up by Puri and Seshadri[42] for an opposed-jet flame was used as the first validation case for these purposes as it provides a good set of experimental data to which the numerical predictions can be compared. A methane-air counter-flow flame was set up using two ducts, each with an inner diameter of 2.54 cm and with a separation distance of 1.4876 cm. The axial velocities of methane and air were 76.8 cm/s

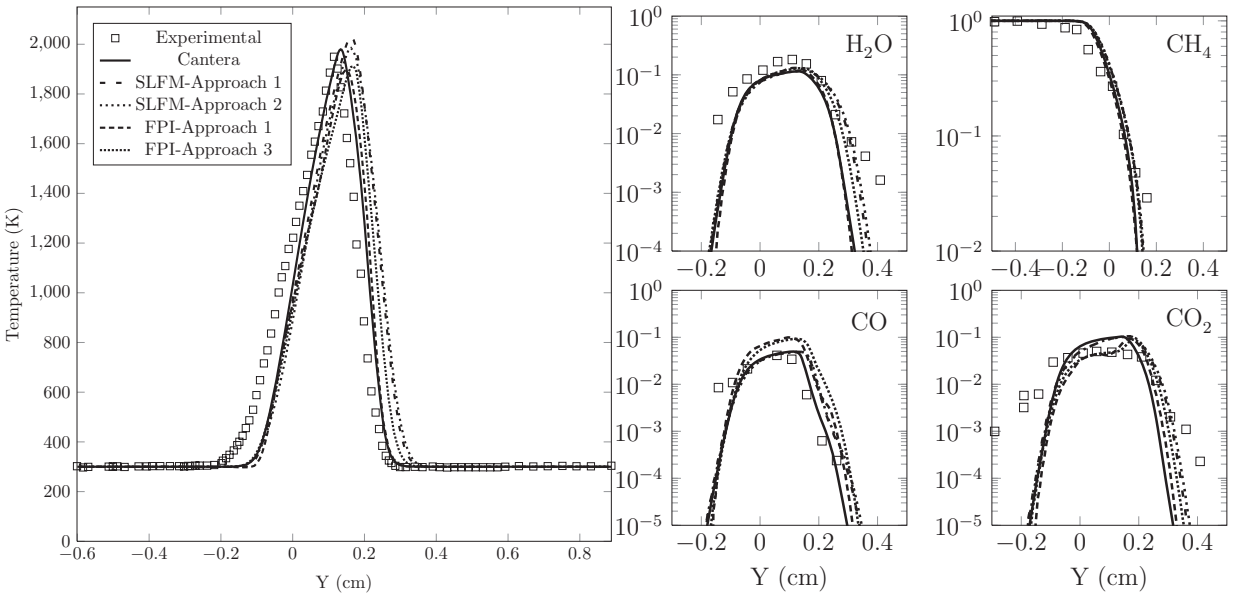

(a) Predicted center-line temperature profiles.

(b) Predicted center-line species concentration profiles.

Figure 7: Comparison of predicted flow profiles and experimental results for the laminar methane-air counter-flow flame.

and 73.4 cm/s, respectively. A number of fine wire screens were placed in the duct to reduce turbulence ensuring a flat laminar velocity profile at the exit of the duct.

The initial grid and boundary conditions used for this problem is shown in Figure 6a. A reflection boundary condition is used on the left boundary representing the symmetry plane. The inflow boundary conditions for both the ducts are kept fixed. All the far-field boundaries are set to constant atmospheric pressure and zero gradient for all other physical properties. The initial grid consists of 30 blocks, each block with 16 by 16 grid points.

After obtaining an initial approximate solution on the coarse grid, two levels of refinement were applied using the AMR capability of the solution method. The final grid for FPI-Approach 3 case after two levels of refinement is depicted in Figure 6b. The refinement criteria was chosen to be the density gradient in order to track the region of maximum chemical activity. The new grid blocks are mostly concentrated halfway between the ducts along the flame. This example for the refined grid shows the potential of the AMR method, in terms of being able to refine areas of maximum activity. It should be noted that the predicted high temperature region in Figure 6b extends somewhat outside the mixing region. This can be attributed to the fact that, in the experimental setup, an inert curtain of N_2 was used. The present numerical implementation was set up to handle only one fuel and one oxidizer stream, i.e., deal with a single mixture fraction variable. To account for another stream of flow, modifications to the present implementation would be needed to account for multiple streams and mixture fractions.

The center-line profiles of temperature and major species predicted by both the SLFM and FPI methods are compared to the experimental data provided by Puri *et al.*[42] in Figures 7a and 7b. It can be seen that all of the tabulation methods reproduce the species and temperature profiles extremely well. The temperature profiles predicted by the tabulation methods however are shifted to the right as compared to the experimental results. The maximum temperature predicted by each numerical approach is summarized in Table 2. The flamelet approaches tend to over-predict the temperature, while the FPI approaches under-predict the temperature by almost the same magnitude. SLFM-Approach 2 has the best agreement with experiment, which is expected as it directly uses the temperature predicted by Cantera for the opposed jet diffusion flame. However, the agreement between tabulated chemistry results and experiment are much better than the one-step mechanism, which over-predicts the temperature by more than 200 K. The preceding results quite clearly demonstrate that the FPI approach can successfully predict a counter-flow flame profile with virtually the same accuracy as the SLFM, a method based entirely on tabulated counter-flow solutions. The results therefore also provide strong justification for the use of the FPI methods based on premixed

Experimental	Cantera	One-Step	FPI-Approach 1	FPI-Approach 3	SLFM-Approach 1	SLFM-Approach 2
1950 K	1980 K	2169 K	1897 K	1912 K	2031 K	1985 K

Table 2: Maximum temperature predicted by different approaches for counter-flow methane-air flame.

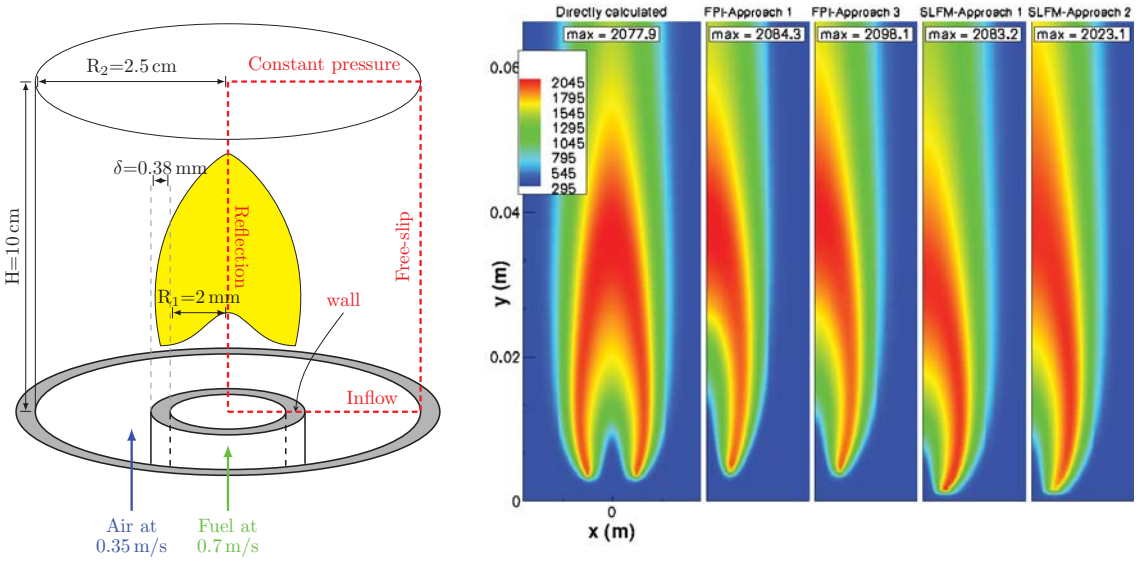

(a) Schematic diagram of the flow geometry and computational domain used in predictions of co-flow laminar diffusion flame.

(b) Predicted distributions of temperature for the methane-air co-flow laminar diffusion flame obtained using direct calculation and tabulated chemistry with the GRI-Mech 3.0 mechanism.

Figure 8: Computational domain and predicted temperature distributions for co-flow laminar diffusion flame.

flamelets in the numerical simulation of more general diffusion flames.

IV.C. Co-Flow Laminar Diffusion Flame

The FPI and SLFM approaches were also compared and assessed when applied to the solution of the steady co-flow laminar diffusion flame studied previously by Mohammed *et al.*,[43] Day and Bell[44] and Northrup and Groth *et al.*[35] Numerical predictions of this axisymmetric flame and burner were obtained on a computational domain that was rectangular in shape with dimensions 10 cm by 2.5 cm, as shown in Figure 8a. The axis of symmetry was aligned with the left boundary and the right far-field boundary was taken to be a free-slip boundary. The top or outlet of the flow domain was open to a stagnant reservoir. The bottom or inlet was divided into three distinct regions. The innermost region was the fuel inlet which injects a nitrogen diluted methane fuel mixture ($Y_{CH_4} = 0.5149$, $Y_{N_2} = 0.4851$) at 298 K with a parabolic velocity profile having a maximum velocity of 0.7 m/s. A second region representing the annular wall separating the fuel and oxidizer streams was followed by a third region containing co-flowing air at 298 K with a uniform velocity of 0.35 m/s. A computational mesh consisting of 18 432 cells was used for which the smallest cell size was about 0.25 mm by 1.4 mm. Simulations were also performed on a coarser mesh containing 3456 cells to assess grid convergence of the solution. Although not shown here, the good agreement found between coarse and fine mesh solutions was felt to be strongly indicative of a near grid converged solution on the fine mesh.

As with the previous laminar flames, both the simple one-step and more detailed GRI-Mech 3.0 reaction mechanisms were considered for this co-flow diffusion flame. For the flame calculations, results were obtained for both mechanisms via direct calculation of the finite-rate chemical kinetics. The FPI tables were constructed using 100 values for Z and 155 values for Y_c for both mechanisms and solution for FPI Approaches 1 and 3 were determined. The SLFM approach was also used to obtain solutions for the detailed chemistry model. Solutions for SLFM Approaches 1 and 2 were determined using a flamelet library storing solutions for 155 values of Z and 18 scalar dissipation rate values.

Predicted distributions of the temperature obtained using direct calculation and tabulated chemistry for

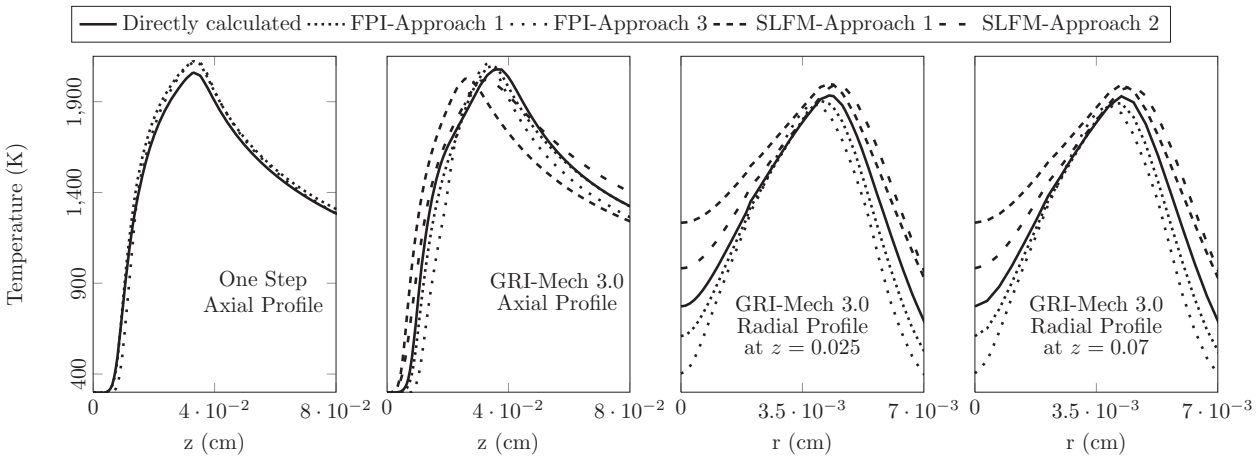

(a) Predicted temperature profiles.

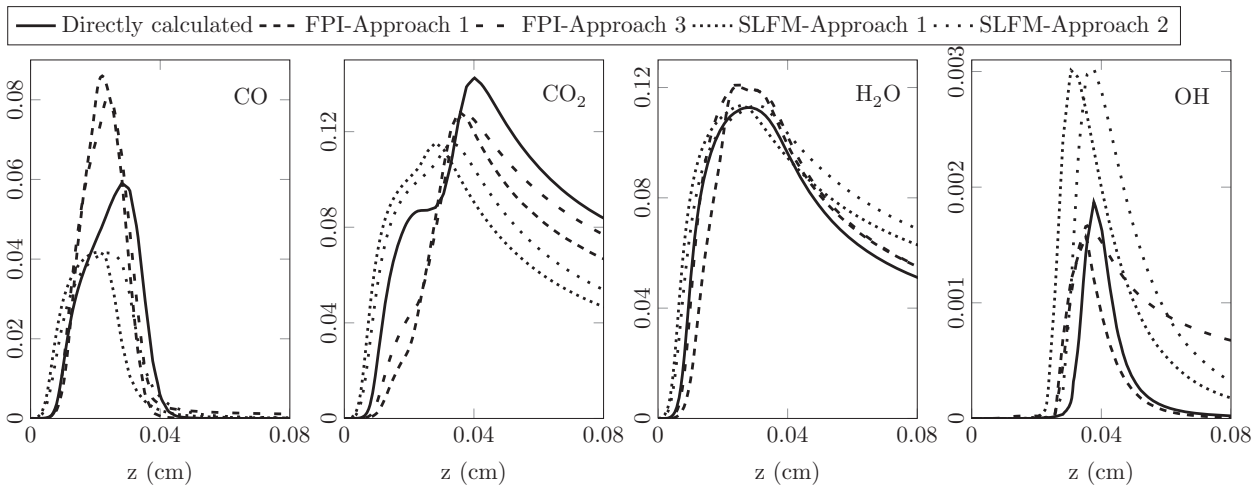

(b) Predicted center-line profiles of species concentration.

Figure 9: Comparison of predicted profiles for the methane-air co-flow laminar diffusion flame obtained using direct-calculation and tabulated chemistry.

FPI Approaches 1 and 3 and SLFM Approaches 1 and 2 with the GRI-Mech 3.0 mechanism are compared in Figure 8b. Furthermore, predicted temperature profiles obtained using both the one-step and detailed chemical mechanisms are shown in Figure 9a. The two figures indicate that the FPI schemes predict the high-temperature regions of the flame much better than does the SLFM approach, for which this region is more spread out when the GRI-Mech 3.0 mechanism is used. The results also show that the predicted centre-line and radial temperature profiles of the directly-calculated solutions are quite accurately recovered by FPI approaches for detailed mechanisms. The SLFM-Approach 1 approach predicts the highest temperature much earlier than all other methods and the high temperature region in the SLFM-Approach 2 extends further downstream higher up in the flame than for the other approaches. It is important to note that the maximum temperature predicted by the detailed-chemistry schemes are much closer to the experimental results reported by Mohammed *et al.*[43] than the results predicted by the one-step mechanism, indicating the importance of finite-rate chemistry for diffusion flames of this type. An accurate balance between transport and chemical reaction rates is needed to predict flame temperature and this cannot be provided by simple one-step mechanisms for the diffusion flame.

Predictions of the mass fraction of some major and minor species are shown in Figure 9b. The FPI approaches reproduce the magnitude and profiles predicted by the detailed-chemistry very well. However, note that OH radical exhibits higher diffusion in the FPI-Approach 3 results. This can be probably attributed to the use of species transport equations only on the reduced set of tabulated species. However, the agreement

	Directly Calculated	FPI Approach 1	FPI Approach 3	SLFM Approach 1	SLFM Approach 2
Size of table	N/A	1.9 MB	1.9 MB	0.069 MB	0.0635 MB
CPU time/iteration	0.0770 (10.84)	0.007 12 (1.03)	0.007 53 (1.09)	0.006 93 (1.0)	0.006 97 (1.001)
% time spent in reading tables	N/A	0.3	0.4	1.0	0.6
% time spent in calculating $\dot{\omega}_i$	43.04	N/A	0.4	N/A	N/A
Predicted flame height	3.56 cm	3.33 cm	3.52 cm	2.61 cm	3.26 cm
Predicted lift-off height	1.15 cm	1.25 cm	1.45 cm	0.08 cm	0.10 cm
Predicted max. temperature	2078 K	2084 K	2098 K	2083 K	2023 K

Table 3: Summary of comparisons of tabulated chemistry methods for methane-air diffusion flame with GRI-Mech 3.0 chemical mechanism.

	Directly Calculated	FPI-Approach 1	FPI-Approach 3
1-step	2181 K	2172 K	2168 K
GRI-Mech 3.0	2077 K	2084 K	2098 K

Table 4: Maximum temperature calculated for the axisymmetric laminar diffusion flame using different numerical and chemical kinetic schemes. The maximum center line temperature reported by Mohammed *et al.*[43] is between 2025 K and 2029 K.

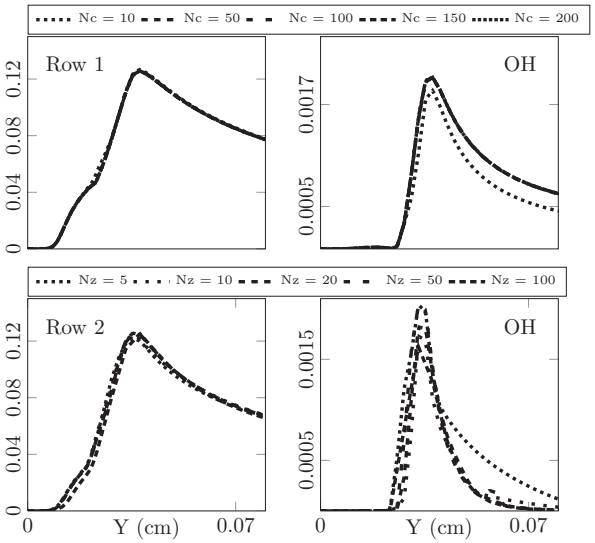

(a) FPI predictions of the profiles of the CO_2 and OH along the center line of the methane-air laminar diffusion flame obtained with GRI-Mech 3.0 chemical mechanism using: (Top, Row 1) different numbers of c points in the FPI-Approach 3 table, (Bottom, Row 2) different number of z points in the FPI-Approach 1 table.

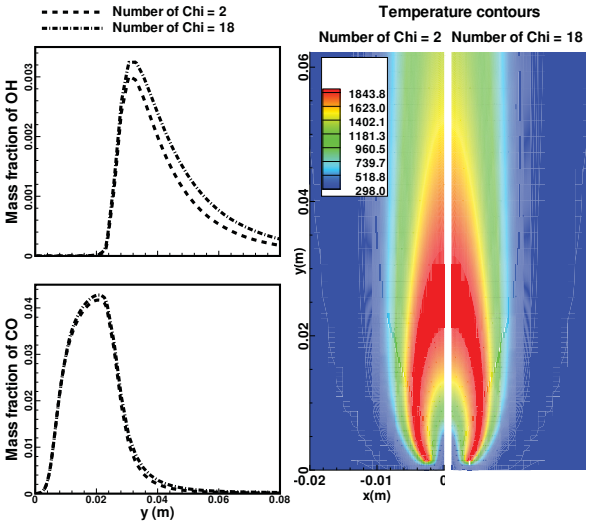

(b) SLFM predictions of the profiles of the mass fractions of OH and CO along the center line and the distribution of the temperature for methane-air laminar diffusion flame obtained using two different flamelet libraries with GRI-Mech 3.0 chemical mechanism.

Figure 10: Effect of table size on numerical results of tabulated chemistry approaches.

between the maximum concentration of OH predicted by the FPI method and direct calculation is much better in comparison to that achieved by the SLFM.

Table 3 provides a detailed summary of the comparisons between the tabulation methods and computational costs involved for the diffusion flame with the detailed GRI-Mech 3.0 mechanism. The advantages of the FPI over the flamelet approaches is again evident when considering some of the global properties of the flame predicted by each scheme. The FPI results are in much better agreement with directly-calculated results for overall flame height and lift-off height. Table 3 also shows that the CPU time per iteration is almost the same for the FPI and flamelet approaches. Moreover, all of these tabulation schemes are almost 11 times faster than directly solving the full set of species balance equations. This is because direct calcu-

	Directly Calculated	FPI-Approach 1	FPI Approach 3
1-step	0.003 96 (1)	0.004 33 (1.09)	0.004 36 (1.1)
GRI-Mech 3.0	0.0770 (19.44)	0.007 12 (1.8)	0.007 53 (1.9)

Table 5: CPU time required per iteration for the axisymmetric laminar diffusion flame. The figure in bracket shows the normalized values.

lation of the reaction rates for the detailed methane-air chemical kinetic mechanism requires almost 43% of the computational time while evaluation and retrieval of tabulated data in the flamelet approaches requires less than 0.4% of the processor time.

In contrast to the results for the detailed mechanism, it is interesting that, for the one-step mechanism, use of the FPI tabulated approaches results in a slightly higher computational cost compared with the cost of the directly-calculated simulation. This is due to the additional overhead associated with interpolating tabulated values that is not offset by a significant reduction in the number of partial differential equations that must be solved. Obviously, the computationally payoffs of tabulation methods can really only be fully realized for larger reaction mechanisms.

Figure 10a provides an indication of how predicted species mass fractions are affected by the size of the FPI tables. The predicted center-line profiles of the mass fractions of both major and minor species are depicted for differing numbers of Z and Y_c points in the FPI tables. It is evident that major species, such as CO_2, are fairly independent of table size. However, for minor species, such as OH, the FPI predictions are more strongly dependent on the size of the table. For table sizes greater than 50 by 100, the results appear to be essentially independent of the tabulation procedure. Similarly, Figure 10b compares the results for two SLFM table sizes: one table built using only two values for the scalar dissipation rate, χ, and the other using 18 different values. Although major species are also not greatly affected by the size of the flamelet library, minor species exhibit slight variations from the directly-calculated results. It would seem for these near equilibrium flames, the SLFM results are not very sensitive to the number of tabulated scalar dissipation rates.

V. Conclusions

The SLFM and the FPI approaches have been compared extensively in the present study for laminar flames. The primary focus was to compare the performance of each approach for laminar diffusion flames. Two flames were studied: the methane-air opposed jet flame and a co-flow laminar diffusion flame. It was found that both FPI and SLFM can be successfully applied to the laminar diffusion flames and reproduce the effects of detail chemistry and predict major and minor species concentrations at a much lower computational cost. The opposed-jet flame study results strongly demonstrate that FPI approaches, based on tabulated solutions of premixed flamelets, are capable of predicting diffusion flame structure as well, if not better, than flamelet approaches, which are based on tabulated solutions of steady diffusion flames. It was also found that SLFM approaches over-predict the concentrations of minor species in most regions of the co-flow flame. Similar findings have been reported in earlier studies of the SLFM approach. Also, the predicted flame height and lift-off-height of the FPI approaches are much closer to the directly-calculated chemistry results than those of the SLFM. The FPI approaches were found to be able to deal more readily with regions of high scalar dissipation rate of mixture fraction. These findings coupled with the ability of FPI approaches to handle both premixed and non-premixed flames, make the FPI tabulated approaches very appealing compared to SLFM approaches. While the concept of FPI tabulation is essentially an *ansatz* (i.e., an educated guess that is later verified by its results), the findings of the present study would certainly lend strong support for its use in the numerical prediction of combustion processes.

The effect of table size on the accuracy of predicted results was also examined. For FPI approaches, very coarse tables successfully reproduce the species concentrations of major species; however, more refined tables are needed to predict the minor species accurately. For the SLFM approach, it was found that for methane-air flames considered herein, the results are not greatly affected by the number of tabulated values used for the scalar dissipation rate.

Future research in this area will be directed to the application of the FPI tabulation method to turbulent flames using a presumed probability density function approach. Comparisons of a presumed conditional moment (PCM) FPI method to other subfilter-scale methods for the large-eddy simulation of turbulent

premixed flames have already been carried out and reported in the recent studies by Perez *et al.*[45]

Acknowledgments

Computational resources for performing the calculations reported herein were provided by the SciNet High Performance Computing Consortium at the University of Toronto and Compute/Calcul Canada through funding from the Canada Foundation for Innovation (CFI) and the Province of Ontario, Canada.

References

[1]Delhaye, S., Sommers, L. M. T., van Oijen, J. A., and de Goey, L. P. H., "Incorporating unsteady flow-effects in flamelet-generated manifolds," *Combustion and Flame*, Vol. 155, 2008, pp. 133–144.

[2]Pope, S. B., "Computationally efficient implementation of combustion chemistry using *in situ* adaptive tabulation," *Combustion Theory and Modelling*, Vol. 1, 1997, pp. 41–63.

[3]Peters, N., "Reducing Mechanisms," 1991.

[4]Oijen, J. A. V. and Goey, L. P. H. D., "Modeling of Premixed Laminar Flames using Flamelet-Generated Manifolds," *Combustion Science and Technology*, Vol. 161, 2000, pp. 113–137.

[5]Lam, S. H. and Goussis, D. A., "Conventional Asymptotics and Computational Singular Perturbation for Simplified Kinetics Modeling," 1991.

[6]Maas, U. and Pope, S. B., "Simplifying Chemical Kinetics: Intrinsic Low-Dimensional Manifolds in Composition Space," *Combustion and Flame*, 1992, pp. 239–264.

[7]Pope, S. B. and Maas, U., "Simplifying chemical kinetics: Trajectory generated low-dimensional manifolds," *Mechanical and Aerospace Engineering Report:FDA 93-11*, 1993.

[8]Wang, M., Huang, J., Frisque, A., and Bushe, W. K., "Generating Trajectories for Low-dimensional Manifolds using the Stochastic Particle Model," *Combustion Theory and Modelling*, Vol. 12, No. 2, 2008, pp. 249–267.

[9]Bilger, R. W., "Turbulent flows with nonpremixed reactants," *Turbulent reacting flows*, 1980, pp. 65–113.

[10]Libby, P. A. and Williams, F. A., "Turbulent Flows Involving Chemical Reactions," *Annual Rev. of Fluid Mechanics*, Vol. 8, 1976, pp. 351–376.

[11]Peters, N., "Laminar Diffusion Flamelet Models in Non-Premixed Turbulent Combustion," *Prog. Energy Combustion Sci.*, Vol. 10, 1984, pp. 319–339.

[12]Chen, M., Herrmann, M., and Peters, N., "Flamelet Modeling Of Lifted Turbulent Methane/Air And Propane/Air Jet Diffusion Flames," *Proceedings of the Combustion Institute*, Vol. 28, 2000, pp. 167–174.

[13]Wen, Z., Yun, S., Thomson, M. J., and Lightstone, M. F., "Modeling Soot Formation in Turbulent Kerosene/Air Jet Diffusion Flames," *Combust. Flame*, Vol. 135, 2003, pp. 323–340.

[14]Liu, F., Guo, H., and Smallwood, G. J., "Evaluation of the laminar diffusion flamelet model in the calculation of an axisymmetric coflow laminar ethylene-air diffusion flame," *Combustion and Flame*, Vol. 144, 2006, pp. 605–618.

[15]Smooke, M. D., Xu, Y., Zurn, R. M., Lin, P., Frank, J. H., and Long, M. B., "Computational And Experimental Study Of OH and CH Radicals In Axisymmetric Laminar Diffusion Flames," *The Combustion Institute*, Vol. 24, 1992, pp. 813–821.

[16]Nishioka, M., Takemoto, Y., Yamashita, H., and Takeno, T., "Effects Of Multi-Dimensionality On A Diffusion Flame," *The Combustion Institute*, Vol. 26, 1996, pp. 1071–1077.

[17]Gicquel, O., Darabiha, N., and Thévenin, D., "Laminar premixed hyrogen/air counterflow flame simulations using flame prolongation of ILDM with differential diffusion," *Proceedings of the Combustion Institute*, Vol. 28, 2000, pp. 1901–1908.

[18]Vervisch, L., Hauguel, R., Domingo, P., and Rullaud, M., "Three facets of turbulent combustion modelling: DNS of premixed V-flame, LES of lifted nonpremixed flame and RANS of jet-flame," *Journal of Turbulence*, Vol. 4, 2004, pp. 1–36.

[19]Fiorina, B., Baron, R., Gicquel, O., Vervisch, L., Carpentier, S., and Darabiha, N., "Modelling non-adiabatic partially premixed flames using flame-prolongation of ILDM," *Combustion Theory and Modelling*, Vol. 7, 2003, pp. 449–470.

[20]Fiorina, B., Gicquel, O., Vervisch, L., Carpentier, S., and Darabiha, N., "Premixed turbulent combustion modeling using tabulated detailed chemistry and PDF," *Proceedings of the Combustion Institute*, Vol. 30, 2005, pp. 867–874.

[21]Galpin, J., Naudin, A., Vervich, L., Christian Angelberger, O. C., and Domingo, P., "Large-eddy simulation of a fuel-lean premixed turbulent swirl-burner," *Combustion and Flame*, Vol. 155, 2008, pp. 247–266.

[22]Oijen, J. A. V., Lammers, F. A., and Goey, L. P. H. D., "Modeling of Complex Premixed Burner Systems by Using Flame-Generated Manifold," *The Combustion Institute*, Vol. 127, 2001, pp. 2124–2134.

[23]Domingo, P., Vervisch, L., and Veynante, D., "Large-Eddy simulation of a lifted methane jet flame in a vitiated coflow," *Combustion and Flame*, Vol. 152, 2008, pp. 415–432.

[24]Michel, J.-B., Colin, O., and Veynante, D., "Comparison of Differing Formulations of the PCM Model by their Application to the Simulation of an Auto-igniting H_2/air jet," *Flow Turbulence Combustion*, 2009, pp. 33–60.

[25]Michel, J.-B., Colin, O., Angelberger, C., and Veynante, D., "Using the tabulated diffusion flamelet model ADF-PCM to simulate a lifted methane-air jet flame," *Combustion and Flame*, Vol. 156, 2009, pp. 1318–1331.

[26]Peters, N., *Turbulent Combustion*, Cambridge University Press, Cambridge, 1st ed., 2000.

[27]Goodwin, D. and Moffat, H. K., "Cantera," http://code.google.com/p/cantera/.

[28]S. K. Liew, K. N. C. B. and Moss, J. B., "A stretched laminar flamelet model of turbulent nonpremixed combustion," *Combustion and Flame*, Vol. 56, 1984, pp. 199.

[29]Domingo, P., Vervisch, L., and Sandra Payet, R. H., "DNS of a premixed turbulent V flame and LES of a ducted flame using a FSD-PDF subgrid scale closure with FPI-tabulated chemistry," *Combustion and Flame*, 2005, pp. 566–586.

[30]Fiorina, B., Gicquel, O., Vervisch, L., Carpentier, S., and Darabiha, N., "Approximating the chemical structure of partially premixed and diffusion counterflow flames using FPI flamelet tabulation," *Combustion and Flame*, Vol. 140, 2005, pp. 147–160.

[31]Galpin, J., *Modélisation LES de la combustion avec une prise en compte des effets de cinétique détaillée et en perspective d'application moteur*, Ph.D. thesis, IFP, Division Techniques d'Applications Énergétiques, September 2007.

[32]Vicquelin, R., Fiorina, B., Payet, S., Darabiha, N., and Gicquel, O., "Coupling tabulated chemistry with compressible CFD solvers," Accepted in the Proceedings of the Combustion Institute, 2011.

[33]Kuo, K., *Principles of Combustion*, John Wiley & Sons, 1986.
[34]Aris, R., *Vectors, Tensors and the Basic Equations of Fluid Mechanics*, Dover Publications, New Jersey, 1989.
[35]Northrup, S. A. and Groth, C. P. T., "Solution of Laminar Diffusion Flames Using a Parallel Adaptive Mesh Refinement Algorithm," Paper 2005–0547, AIAA, January 2005.
[36]Gao, X. and Groth, C. P. T., "Parallel Adaptive Mesh Refinement Scheme for Turbulent Non-Premixed Combusting Flow Prediction," Paper 2006-1448, AIAA, January 2006.
[37]Gao, X. and Groth, C. P. T., "A Parallel Adaptive Mesh Refinement Algorithm for Predicting Turbulent Non-Premixed Combusting Flows," *Int. J. Comput. Fluid Dyn.*, Vol. 20, No. 5, 2006, pp. 349–357.
[38]Charest, M. R. J., Groth, C. P. T., and Gülder, O. L., "A computational framework for solving laminar reacting flows with soot formation," *Combustion Theory and Modelling*, Vol. 14, No. 6, 2010, pp. 793–825.
[39]Westbrook, C. K. and Dryer, F. L., "Simplified Reaction Mechanisms for the Oxidation of Hydrocarbon Fuels in Flames," *Combust. Sci. Tech.*, Vol. 27, 1981, pp. 31–43.
[40]Smith, G. P., Golden, D. M., Frenklach, M., Moriarty, N. W., Eiteneer, B., Goldenberg, M., Bowman, C. T., Hanson, R. K., Song, S., Gardiner, W. C., Lissianski, V. V., and Qin, Z., "GRI-Mech 3.0," http://www.me.berkeley.edu/gri_mech/.
[41]Gao, X., Northrup, S., and Groth, C. P. T., "Parallel solution-adaptive method for two-dimensional non-premixed combusting flows," accepted in the Progress in Computational Fluid Dynamics, 2010.
[42]Puri, I. K., Seshadri, K., Smooke, M. D., and Keyes, D. E., "A Comparison Between Numerical Calculations and Experimental Measurements of the Structure of a Counterflow Methane-Air Diffusion Flame," *Combustion Science and Technology*, Vol. 56, 1987, pp. 1–22.
[43]Mohammed, R. K., Tanoff, M. A., Smooke, M. D., Schaffer, A. M., and Long, M. B., "Computational and Experimental Study of a Forced, Time-Varying, Axisymmetric, Laminar Diffusion Flame," *Twenty-Seventh Symposium (International) on Combustion*, The Combustion Institute, Pittsburgh, 1998, pp. 693–702.
[44]Bell, J., Day, M., Almgren, A., Lijewski, M. J., and Rendleman, C. A., "Adaptive Numerical Simulation of Turbulent Premixed Combustion," *Proceedings of the First MIT Conference on Computational Fluid and Solid Mechanics*, June 2001, p. 1.
[45]F.E.Hernàndez-Pérez, Yuen, F., Groth, C., and Ö.L.Gulder, "LES of a laboratory-scale turbulent premixed Bunsen flame using FSD, PCM-FPI and thickened flame models," accepted in the Proceedings of the Combustion Institute, doi:10.1016/j.proci.2010.06.010., 2010.